Journal of Materials Chemistry A

Plasmonic Ag-Decorated Few-Layer MoS_2 Nanosheets Vertically Grown on Graphene for Efficient Photoelectrochemical Water Splitting

Journal:	*Journal of Materials Chemistry A*
Manuscript ID	TA-ART-04-2020-004529
Article Type:	Paper
Date Submitted by the Author:	30-Apr-2020
Complete List of Authors:	Seo, Dong-Bum; Chungnam National University, Department of Materials Science & Engineering Trung, Tran Nam; Quy Nhon University, Department of Physics & Materials Science, Faculty of Natural Sciences Kim, Dong-Ok; Chungnam National University, Department of Materials Science & Engineering Duc, Duong Viet; Chungnam National University, Department of Materials Science & Engineering Jeong, Jong-Ryul; Chungnam National Univ., Dept. of Mater. Sci. & Eng., Graduate School of Green Energy Tech. Kim, Eui-Tae; Chungnam National University, Department of Materials Science & Engineering

Journal of Materials Chemistry A
Materials for energy and sustainability

Guidelines for Reviewers

Thank you very much for agreeing to review this manuscript for *Journal of Materials Chemistry A*.

Journal of Materials Chemistry A is a weekly journal in the materials field. The journal is interdisciplinary, publishing work of international significance on all aspects of materials chemistry related to applications in energy and sustainability. Articles cover the fabrication, properties and applications of materials.

Journal of Materials Chemistry A's Impact Factor is **10.733** (2018 Journal Citation Reports®)

The following manuscript has been submitted for consideration as a

FULL PAPER

For acceptance, a Full Paper must report primary research that demonstrates significant **novelty and advance**, either in the chemistry used to produce materials or in the properties/ applications of the materials produced. Work submitted that is outside of these criteria will not usually be considered for publication. The materials should also be related to the theme of energy and sustainability.

When preparing your report, please:

- Focus on the **originality**, **importance**, **impact** and **reproducibility** of the science.
- Refer to the **journal scope and expectations**.
- **State clearly** whether you think the article should be accepted or rejected and give detailed comments (with references) both to help the Editor to make a decision on the paper and the authors to improve it.
- **Inform the Editor** if there is a conflict of interest, a significant part of the work you cannot review with confidence or if parts of the work have previously been published.
- **Provide your report rapidly** or inform the Editor if you are unable to do so.

Best regards,

Professor Anders Hagfeldt
Editor-in-Chief
EPFL, Switzerland

Dr Sam Keltie
Executive Editor
Royal Society of Chemistry

Contact us

Please visit our reviewer hub for further details of our processes, policies and reviewer responsibilities as well as guidance on how to review, or click the links below.

What to do when you review

Reviewer responsibilities

Process & policies

DEPARTMENT OF MATERIALS SCIENCE & ENGINEERING
CHUNGNAM NATIONAL UNIVERSITY

99 DAEHAK-RO, DAEJEON 34134, KOREA
Tel. +82-42-821-6631 Fax. +82-42-822-5850 http://mateng.cnu.ac.kr

April 30, 2020

Dear Editor,

Please find enclosed our manuscript entitled "Plasmonic Ag-Decorated Few-Layer MoS_2 Nanosheets Vertically Grown on Graphene for Efficient Photoelectrochemical Water Splitting", which we would like you to consider for publication of a *Full paper* in *Journal of Materials Chemistry A*.

A controllable and practical large-scale approach that combines surface plasmon resonance (SPR) and two-dimensional (2D) graphene/MoS_2 heterojunction has not been implemented despite its potential for efficient photoelectrochemical (PEC) water splitting. In this study, plasmonic Ag-decorated 2D MoS_2 nanosheets were vertically grown on graphene substrates through metalorganic chemical vapor deposition of MoS_2 and thermal evaporation of Ag. The PEC performance of MoS_2 was significantly enhanced by the synergetic effects of (i) SPR-enhanced optical absorption and photo generation of charge carriers and (ii) efficient separation and transportation of photo-generated e–h pairs through few-layer MoS_2 nanosheets that are vertically-aligned on graphene. This study provides a promising path for exploiting the full potential of 2D MoS_2 for practical large-scale and efficient PEC applications.

This manuscript has not been published elsewhere and is not under consideration by another journal. We have approved the manuscript and agree with submission to *Journal of Materials Chemistry A*. There are no conflicts of interest to declare. We believe that the findings of this study are relevant to the scope of your journal and will be of interest to its readership.

I look forward to hearing from you at your earliest convenience.
Thank you.

Sincerely,

Eui-Tae Kim, Ph.D.
Professor
Department of Materials Science & Engineering
Chungnam National University
Daejeon, 305-764, Korea
E-mail: etkim@cnu.ac.kr
Tel: +82 42-821-5895

Plasmonic Ag-Decorated Few-Layer MoS_2 Nanosheets Vertically Grown on Graphene for Efficient Photoelectrochemical Water Splitting

Dong-Bum Seo, Tran Nam Trung, Dong-Ok Kim, Duong Viet Duc, Jong-Ryul Jeong, and Eui-Tae Kim*

Department of Materials Science & Engineering, Chungnam National University, Daejeon 34134, Republic of Korea

* Corresponding author. E-mail: etkim@cnu.ac.kr

A controllable approach that combines surface plasmon resonance (SPR) and two-dimensional (2D) graphene/MoS_2 heterojunction has not been implemented despite its potential for efficient photoelectrochemical (PEC) water splitting. In this study, plasmonic Ag-decorated 2D MoS_2 nanosheets were vertically grown on graphene substrates in a practical large-scale manner through metalorganic chemical vapor deposition of MoS_2 and thermal evaporation of Ag. The plasmonic Ag-decorated MoS_2 nanosheets on graphene yielded up to 10 times higher photo to dark current ratio than MoS_2 nanosheets on indium-tin oxide. The significantly enhanced PEC activity could be attributed to the synergetic effects of SPR and favorable graphene/2D MoS_2 heterojunction. Plasmonic Ag NPs not only increased visible-light and near-infrared absorption of 2D MoS_2 but also induced highly amplified local electric field intensity in 2D MoS_2. In addition, the vertically aligned 2D MoS_2 on graphene acted as a desirable heterostructure for efficient separation and transportation of photo-generated carriers. This study provides a promising path for exploiting the full potential of 2D MoS_2 for practical large-scale and efficient PEC water-splitting applications.

Keywords: Photoelectrocatalysis, molybdenum disulfide, graphene, surface plasmon resonance

1. Introduction

Photoelectrochemical (PEC) water splitting has been extensively studied as an effective approach for converting solar energy into chemical fuel, such as hydrogen gas.[1-4] Recently, two-dimensional (2D) layered MoS_2 has attracted considerable research attention as a promising semiconductor photocatalyst because of its excellent catalytic activity, high chemical stability, eco-friendliness, and abundance in nature.[2-4] In particular, few-layer thick MoS_2 nanosheets can be central to exploiting the full potential of 2D MoS_2 for solar-light PEC reactions because of the feasibility of mass production and appropriate bandgap energy, which is tunable from ~1.2 eV for indirect gap in the bulk form to ~1.9 eV for direct gap in the monolayer.[5-7] The PEC activity of 2D MoS_2, which has strong in-plane covalent bonding of S–Mo–S and weak out-of-plane van der Waals interaction between neighboring S–S layers, is significantly hindered by poor charge transport across basal layers through hopping.[2-4] Thus, the ideal architecture configuration comprises 2D MoS_2 nanosheets that stand vertically on electrode substrates because the highly conductive edges of MoS_2 provide an efficient pathway for photo-excited carriers and good electronic contact with the substrate. In addition, vertically packed 2D sheets offer higher volume than laid sheets for interacting with incoming photon flux on a unit substrate area. He et al.[8] demonstrated that the edge-on structure of MoS_2 flakes/TiO_2 nanowires improves the photocatalytic hydrogen evolution of MoS_2. Recently, we reported the enhanced PEC activity of few-layer MoS_2 nanosheets vertically grown on supporting electrode substrates, such as indium-tin oxide (ITO) and ITO/TiO_2 nanowires.[9,10] However, the synthesis and PEC applications of vertically aligned few-layer MoS_2 nanosheets on graphene have not been reported yet despite its considerable potential.

The support substrate should be made highly conductive and form an appropriate energy band alignment with MoS_2 to minimize Ohmic junction losses. Graphene has attracted huge research attention as a promising conducting layer not only because it displays remarkable electron mobility (>15,000 $cm^2 \cdot V^{-1} \cdot s^{-1}$) but also due to its favorable electric contact with MoS_2. Chang et al.[11] reported

the enhanced photocatalytic hydrogen evolution of MoS_2/graphene as a result of the improved charge transport of graphene. Carraro et al.[12] demonstrated the one-pot aerosol synthesis of MoS_2 nanoparticles/graphene for enhanced PEC hydrogen production. Biroju et al.[13] also reported that an adequate stacking of 2D MoS_2 and graphene exhibited a ΔG_H value that is close to zero, which is ideal for hydrogen evolution reactions. However, most MoS_2/graphene heterostructures have been synthesized by wet-chemical and mechanical transfer approaches, which are unsuitable for controlled synthesis or vertical stacking of few-layer MoS_2 nanosheets on graphene electrode substrates.[11-15] Wet-chemical synthesis methods have yielded a wide range of MoS_2 layer thicknesses and produced the randomly assembled structures of 2D MoS_2 and graphene.[11,12,16]

The optical absorption of 2D MoS_2 can be remarkably enhanced by employing plasmonic metal nanoparticles (NPs), such as Ag or Au. Plasmonic metals improve the optical absorption over the entire solar spectrum as well as broaden and tune the optical absorption behavior, depending on their composition, size, and shape.[17,18] Ag and Au have gained research interest because of their strong resonance with ultraviolet (UV) and visible light. Moreover, the surface plasmon resonance (SPR) of metal NPs enhances the intensity of the electric field near the metal NPs, thereby significantly increasing the rate of electron–hole (e–h) pair generation.[17,19] Plasmonic metal NPs also act as dye sensitizers by absorbing resonant photons and injecting high-energy electrons into the nearby semiconductor.[17,20] Kang et al.[21] reported the effective injection of SPR-excited electrons, i.e., hot electrons, by Au NPs into the conduction band of MoS_2 by overcoming the Schottky barrier (~0.8 eV) of Au/MoS_2. SPR-induced charge carriers should be efficiently transported to the corresponding electrode/water interfaces to maximize the SPR effects and enhance the PEC activity. Vertically aligned few-layer MoS_2 nanosheets on graphene can act as desirable heterostructures to synergistically exploit the SPR effects in terms of energy band diagram and physical nanostructure architecture.

Herein, we report significantly improved PEC efficiency through the synergetic effects of (i) SPR-enhanced optical absorption and photo generation of charge carriers and (ii) efficient separation and transportation of photo-generated e–h pairs through few-layer MoS_2 sheets that are vertically-aligned on graphene. Few-layer MoS_2 sheets were vertically grown on graphene in a controlled manner at relatively low temperatures (250℃) through metalorganic chemical vapor deposition (MOCVD) to minimize damage to the graphene. For the SPR effect, Ag NPs were formed on 2D MoS_2 sheets on graphene through simple thermal evaporation of Ag (Figure 1). Thermal evaporation is a low-cost and practical method for large-area substrates in comparison with previously reported methods, such as sophisticated metal nanopatterning,[18] drop/spin casting of pre-synthesized metal NPs,[22] and chemical synthesis.[19] Ag was chosen as plasmonic metal because of its appropriate resonant wavelength range in the UV to near-infrared (IR) band and smaller work function (~4.3–4.8 eV) than Au (~5.1–5.5 eV) and Pt (~5.1–5.9 eV). Thus, Ag/MoS_2 forms a low Schottky barrier, which is advantageous for the efficient injection of SPR-excited electrons into the conduction band of MoS_2.

2. Experimental

2.1. Preparation of heterostructures of graphene/2D MoS_2/Ag NPs

Graphene was synthesized on Cu foils (Alfa Aesar) by using inductively-coupled plasma (ICP) CVD with CH_4 and H_2 gases at 950℃ for 5 min. The ICP power and growth pressure were fixed at 200 W and 1 Torr, respectively. The synthesized graphene on Cu was transferred on an ITO glass substrate (Figure 1). The CVD growth and transfer procedures of graphene were further described elsewhere.[23] MoS_2 was directly grown on ITO and ITO/graphene at 250℃ by using MOCVD with $Mo(CO)_6$ and H_2S gas (5 vol% in balance N_2) as Mo and S precursors, respectively. $Mo(CO)_6$ was vaporized at 20°C and transferred into a quartz reaction tube with Ar gas of 25 standard cubic centimeters per minute (SCCM). The flow rate of H_2S gas was 75 SCCM. The growth pressure and time were fixed at 1 Torr

and 5 min, respectively. Ag NPs were formed on ITO/graphene/MoS_2 through thermal evaporation of Ag at room temperature. The size and coverage of Ag NPs on few-layer MoS_2 were controlled by various nominal Ag deposition thicknesses of 2, 4, and 8 nm.

2.2. Characterization

The morphology of the samples was investigated via scanning electron microscopy (SEM; Hitachi S-4800) and transmission electron microscopy (TEM; Tecnai G^2 F30 S-Twin). The structural properties of MoS_2 were characterized by TEM and micro-Raman spectroscopy by using an excitation band of 532 nm and a charge-coupled device detector. The chemical states and composition of the samples were characterized by X-ray photoelectron spectroscopy (XPS; Thermo Fisher K-Alpha+). Optical properties were evaluated by UV–visible (UV–Vis; Scinco S-3100) and photoluminescence (PL) spectroscopy (excitation at 532 nm). Photo-excited carrier behavior was investigated by time-resolved PL (TRPL) measurements. The samples were excited using a 467 nm pulsed laser, and the transient signal was recorded using a time-correlated single-photon counting spectrometer (Horiba Fluorolog 3). The energy level of MoS_2 was evaluated via UV photoelectron spectroscopy (UPS; Thermo scientific, K-alpha$^+$).

2.3. Photoelectrochemical measurement

PEC cells were fabricated on 1 × 2 cm^2 ITO glass substrates. The working area of the PEC cells was fixed at 0.5 × 0.5 cm^2 by using non-conductive epoxy to cover the undesired areas. PEC characterization was performed using a three-electrode system and an electrochemical analyzer (potentiostat/galvanostat 263A). A Pt plate and KCl-saturated calomel (Hg/Hg_2Cl_2) were used as counter and reference electrodes, respectively. The electrolyte solutions were prepared with 0.3 M KH_2PO_4 + 0.3 M KOH and 0.5 M Na_2SO_3 + 0.5 M Na_2SO_4. The light source was simulated AM 1.5G

irradiation of 100 mW/cm^2 delivered by a 150 W Xe arc lamp. The current density–voltage characteristics were recorded using a source meter (Keithley 2400). Electrochemical impedance spectroscopy (EIS) measurement was performed under constant light illumination (100 mW/cm^2) at a bias of 0.6 V with varying AC frequencies from 100 kHz to 100 mHz.

3. Results and Discussion

3.1. Microstructure of Ag-NP-decorated MoS_2 nanosheets on graphene

MoS_2 nanosheets with a height of ~200 nm and length of ~150–250 nm were vertically aligned and densely packed on the ITO/graphene substrate (hereinafter referred to as G/MoS_2, Figures 2a and 2b). Owing to the low-temperature growth at 250℃, the graphene layer remained after the MOCVD growth of MoS_2, as confirmed by the presence of the characteristic G and 2D band peaks in the Raman spectrum (inset of Figure 2a). The pristine CVD-grown graphene layer exhibited a low-intensity ratio of D to G band peaks (> 0.15) and an excellent light transmittance of 96.8 % at 550 nm (Figure S1 in Supporting Information), corresponding to approximately one and a half layers of high-quality graphene.[23] The structure of few-layer MoS_2 was investigated using TEM and Raman spectroscopy. The planar-view TEM image of G/MoS_2 clearly showed the layered structure of MoS_2 sheets with edges on graphene (Figure 2c). The sheets comprised 1–5 layers with an interlayer spacing of 0.63 nm, corresponding to the semiconducting 2H MoS_2. The TEM results are consistent with the Raman spectrum of G/MoS_2 (Figure S2a). The E^1_{2g} and A_{1g} modes can be attributed to the in-plane vibration of Mo and S atoms and the out-of-plane vibration of S atoms, respectively. The positions and relative frequency difference (RFD) of E^1_{2g} and the A_{1g} peaks are strongly correlated with the number of MoS_2 layers.[9,24,25] For G/MoS_2, the RFD value (22.3 cm^{-1}) of E^1_{2g} (385.0 cm^{-1}) and A_{1g} peaks (407.3 cm^{-1}) corresponds to a few layers of MoS_2. The MoS_2 sheets grown on ITO (hereinafter referred to as ITO/MoS_2) showed similar size and morphology as the counterpart sample, namely, G/MoS_2 (Figure

S2b). The RED value of E^1_{2g} and A_{1g} peaks of ITO/MoS_2 was also similar to that of G/MoS_2 (Figure S2a).

Figures 2d, 2e, and 2f show the TEM images of Ag-decorated G/MoS_2 with nominal Ag thicknesses of 2, 4, and 8 nm, respectively (referred to as G/MoS_2/Ag-2, G/MoS_2/Ag-4, and G/MoS_2/Ag-8, respectively). The size of the Ag NPs on MoS_2 was successfully manipulated by varying the nominal deposition thickness of Ag through thermal evaporation. For G/MoS_2/Ag-2, Ag NPs with size of ~3–5 nm were formed on the MoS_2 nanosheet surface. The NP size increased to ~10–20 nm for G/MoS_2/Ag-4. By increasing the nominal deposition thickness to 8 nm, the size of Ag NPs increased to ~20–40 nm. In addition, large Ag clusters of ~60–100 nm were partially formed. The high-resolution TEM lattice image revealed that the NPs were metallic Ag (Figure 2g). The metallic Ag was also confirmed by XPS. Figure 3a shows two strong peaks in the XPS spectrum of G/MoS_2/Ag-4 at 373.9 and 367.9 eV, which can be attributed to the Ag $3d_{3/2}$ and Ag $3d_{5/2}$ orbitals of metallic Ag, respectively.[26]

MoS_2 presents two common structure polymorphs, namely, semiconducting 2H and metallic 1T phases, which can be converted from each other by surface treatments, such as Ar-plasma bombardment and metal deposition.[2,27,28] As shown in Figure 3b, the XPS spectra of the Mo 3d core level were deconvoluted into only two peaks at 229.1 and 232.2 eV, which can be attributed to the Mo^{4+} $3d_{5/2}$ and Mo^{4+} $3d_{3/2}$ components of the 2H phase of MoS_2, respectively.[2,27,28] Pristine MoS_2 (G/MoS_2) and Ag NP-decorated MoS_2 (G/MoS_2/Ag-4) exhibited nearly identical XPS spectra at the Mo 3d core level, indicating that the single phase of semiconducting 2H MoS_2 remained stable after Ag NP decoration. This structural stability is highly advantageous for 2D MoS_2 in semiconducting photoelectrode applications. Figure 3c shows the XPS spectra of the S 2p core level of MoS_2. The spectra were deconvoluted into two peaks at 163.2 and 162.0 eV, corresponding to the S $2p_{1/2}$ and S $2p_{3/2}$ orbital of divalent sulfur, respectively.[27] The ratios of the S $2p_{1/2}$ and S $2p_{3/2}$ peaks of G/MoS_2 and G/MoS_2/Ag-

4 were almost identical, suggesting a single phase of 2H MoS_2 for both samples. The 2H phase of both samples was also confirmed by TEM (Figure 2c). G/MoS_2/Ag-4 exhibited a small broad bump near 168 eV, which can be attributed to S^{4+} due to Ag sulfurization. However, the peak was removed by slight Ar-plasma surface etching, indicating the ultrathin layer of silver sulfide.

3.2. Effect of graphene on the PEC activity of MoS_2 nanosheets

The G/MoS_2 and ITO/MoS_2 samples exhibited a PL peak at 676 nm (inset of Figure 4a), which is consistent with the energy of exciton A. Hence, the dominant electronic transition was the direct bandgap transitions at the *K* point.[9] Notably, G/MoS_2 achieved significantly lower PL efficiencies than ITO/MoS_2. The PL quenching efficiency indicated that the graphene layer played a crucial role in reducing the e–h recombination in MoS_2. TRPL spectroscopy study was conducted to further understand the dynamic behavior of photo-generated carriers (Figure 4a). The average carrier lifetimes were extracted using the PL decay kinetics fitted by a bi-exponential decay profile.[29] G/MoS_2 exhibited a shorter carrier lifetime of 3.1 ns than ITO/MoS_2 (4.2 ns). The reduced carrier lifetime can be attributed to the benefits of graphene/MoS_2 heterojunction for efficient separation and transportation of photo-generated carriers to the semiconductor/liquid interface.[15]

EIS study was conducted to further understand the charge transport property. Figure 4b shows the Nyquist plots of EIS in the dark and under illumination. G/MoS_2 exhibited smaller EIS semicircles than ITO/MoS_2, whose radius mirrors the charge transfer resistance (R_{ct}). The Nyquist plots were fitted using a simplified Randles circuit (inset in Figure 4b), consisting of R_{ct}, solution resistance (R_s), constant phase element (Q), and diffusion of species in electrolyte solution represented by Warburg impedance (W). The R_{ct} values are listed in the Supporting Information (Table S1). G/MoS_2 had R_{ct} values of 3,264 and 1,959 Ω, whereas ITO/MoS_2 exhibited R_{ct} values of 4,236 and 2,766 Ω in the dark and under illumination, respectively. Moreover, the R_{ct} (dark) to R_{ct} (photo) ratio (1.67) of G/MoS_2 was greater

than that of ITO/MoS_2 (1.53), suggesting that the photo-generated e–h pairs were efficiently separated and transported through the graphene/MoS_2 heterojunction.

Considering the benefits of graphene/MoS_2 heterojunction, G/MoS_2 exhibited significantly higher PEC activity through the measured potential range than ITO/MoS_2 (Figure 4c). G/MoS_2 yielded approximately nine times higher photocurrent density (1.72 mA/cm^2) at 0.4 V (at which the photo to dark current ratio (I_{ph}/I_{dark}) was at maximum) than ITO/MoS_2 (0.19 mA/cm^2). The maximum I_{ph}/I_{dark} value of G/MoS_2 was approximately 16 at 0.4 V, whereas that of ITO/MoS_2 was approximately 4 at 0.8 V. The water oxidation onset potential (~0.13 V), which is generally defined by the potential at the intersection of the dark current and the tangent at the maximum slope of the photocurrent, of G/MoS_2 had a cathodic shift of ~0.41 V with respect to that (~0.54 V) of ITO/MoS_2. The rapidly increasing photocurrent density of the samples above 0.6 V resulted from the considerably high dark current, which can be attributed to the electrocatalysis and electro-corrosion of MoS_2, in which active S atoms can react with redox species in the solution.[9,11]

3.3. Effect of plasmonic Ag NPs on the PEC activity of graphene/MoS_2 nanosheets

Raman spectroscopy characterization was performed to investigate the interaction of Ag NPs with MoS_2. The characteristic E^1_{2g} and A_{1g} modes of the Ag-decorated samples were red-shifted with respect to those of G/MoS_2-250 because of the stiffening of E^1_{2g} and A_{1g} vibrations (Figure 5a). The stiffened lateral vibration between Mo and S atoms through E^1_{2g} mode resulted from the p-doping effect of Ag NPs in MoS_2.[27] MoS_2/Ag was very likely to form a Schottky junction because of electron transfer from MoS_2 to Ag NPs, as shown in Figure S3. The stiffened vertical vibration of S atoms through A_{1g} mode, was also attributed to the interaction between the Ag NPs and MoS_2.[20] Figure 5b shows the UV–Vis absorption spectra of G/MoS_2 and the Ag-decorated MoS_2 samples. All samples showed two prominent absorption peaks at approximately 607 and 663 nm. The two peaks, known as excitons B and A,

respectively, can be attributed to the direct excitonic transitions at the *K* point of the MoS_2 Brillouin zone.[9,30] In comparison with G/MoS_2, the Ag-decorated MoS_2 samples exhibited stronger absorption intensity, especially for red light and near IR regions. Additionally, the absorption edges (~800 nm) of Ag-decorated MoS_2 samples were red-shifted with respect to that (~750 nm) of G/MoS_2. The enhanced visible light and broadened absorption near the IR region can be attributed to the strong coupling between the excitons and surface plasmons of Ag NPs.[17,18] The PL spectra also exhibited red-shifting behavior with increasing Ag NP sizes (Figure S4). G/MoS_2 showed a PL peak position of 676 nm, corresponding to the energy of the exciton A, representing the direct bandgap transitions at the *K* point of 2D MoS_2. With increasing Ag NP sizes, the PL peak was gradually red-shifted, reaching 688 nm for G/MoS_2/Ag-8.

TRPL study was conducted to investigate the plasmonic effect of Ag NPs on the dynamic carrier behavior. G/MoS_2 exhibited the shortest carrier lifetime of 3.1 ns, whereas G/MoS_2/Ag-4 and G/MoS_2/Ag-8 yielded longer carrier lifetimes of ~3.8 ns (Figure 5c). The carrier lifetime increased with increasing nominal Ag deposition thicknesses. The long carrier lifetimes of Ag-decorated MoS_2 samples can be attributed to suppressed e–h recombination by filling the trapping sites of MoS_2 by plasmon-excited electrons.[20] Ag-decorated MoS_2 samples also exhibited smaller EIS semicircles than G/MoS_2, (Figure 5d and S5). The Nyquist plots of G/MoS_2/Ag-4 yielded the lowest R_{ct} in the dark (~2,572 Ω) and under illumination (~1,284 Ω), suggesting the effective assistance of the carrier transfer through the Ag NPs on the MoS_2 surface. Moreover, G/MoS_2/Ag-4 yielded the highest R_{ct} (dark)/R_{ct} (photo) of 2.00 (inset in Figure 5d). The increased R_{ct} (dark)/R_{ct} (photo) can result from the SPR-enhanced photo-generation and transfer rate of the charge carriers.

To validate the experimental findings, finite-difference time-domain (FDTD) simulations of the interaction of materials with the incident electromagnetic radiation were performed based on Maxwell's equations. Ag hemispheres in an open-air environment under the illumination of a plane-wave source

were considered (Figure S6). A 2D periodic orientation of the NPs on a three-layer-thick MoS_2 substrate was assumed including the following: (i) 3 nm-diameter NPs with a pitch of 20 nm (referred to as AgNP-3), (ii) 15 nm-diameter NPs with a pitch of 30 nm (referred to as AgNP-15), and (iii) 60 nm-diameter NPs with a pitch of 65 nm (referred to as AgNP-60). The electric-field vector of the source oscillated along the *x*-axis, while the propagation vector is along the *z*-axis. Figure 6 shows the simulated UV–Vis absorption spectra and electric field distribution contour plots at the wavelength of SPR (λ_{SPR}) for AgNP-3, AgNP-15, and AgNP-60. The simulated UV–Vis absorption spectrum of pristine MoS_2 substrate was in good agreement with the corresponding experimental result (Figure 6a). The light absorption was significantly enhanced in the visible light and IR regions by Ag NP decoration. Notably, the SPR peaks appeared above the absorption edge of pristine MoS_2 (~700 nm), consistent with the experimentally observed broadened absorption near the IR region. AgNP-15 exhibited the strongest SPR effect, resulting in the highly amplified local electric field intensity in MoS_2 (Figure 6b). The SPR-enhanced electric field can increase the rate of e–h pair generation by a few orders of magnitude.[17] The 15 nm Ag NPs induced an SPR-enhanced electric field in the entire interface region of MoS_2/Ag NP. By contrast, the 60 nm Ag NPs showed SPR effect only along the edge of NPs (Figure 6c), indicating that a significant amount of light was extinguished by big Ag clusters (~60–100 nm) of G/MoS_2/Ag-8 without photogeneration of e–h pairs in MoS_2. In addition, the surface plasmons of small Ag NPs (<30 nm) undergo decay because of the formation of energetic charge carriers, but those of large Ag NPs (>50 nm) undergo decay through the radiative scattering of resonant photons.[26,31] Thus, the Ag NPs of G/MoS_2/Ag-4 efficiently injected SPR-excited electrons into the conduction band of MoS_2, resulting in the largest R_{ct} (dark)/R_{ct} (photo). Meanwhile, the SPR effect of G/MoS_2/Ag-2 was relatively weak because of its low surface coverage of tiny Ag NPs of less than 10 nm (Figure 6a).

To gain insight into the carrier transport property across the heterojunction of graphene/MoS_2, its electronic structure was studied by UPS. The work function of MoS_2 (4.82 ± 0.15 eV) was determined

based on the difference between the photon energy of excited radiation (21.2 eV) and the spectrum width which is measured from the valence band and secondary edges (16.38 eV, Figure 7a). The energy difference between the Fermi energy and valence band edge (E_F-E_{VB}) was 1.36 eV (Figure 7b). Considering the bandgap energy of ~1.88 eV for MoS_2 based on the UV–Vis absorption and PL spectra, the electron affinity of MoS_2 was approximately 4.33 eV, which is consistent with the previously reported values (~4.3 eV).[32] This electronic structure suggests the n-type behavior of MoS_2, working as a photoanode. As shown in Figure 7c, the Fermi level (~4.6–4.8 eV of work function)[33] of pristine few-layer graphene was appropriately located between the Fermi level of the ITO and the conduction band edge of MoS_2 for efficient extraction of electrons to the cathode.

Figure 8a shows the linear sweep voltammograms of G/MoS_2, G/MoS_2/Ag-2, G/MoS_2/Ag-4, and G/MoS_2/Ag-8 under illumination. The Ag-decorated MoS_2 samples exhibited significantly higher PEC activities than G/MoS_2, whereas the dark currents were almost identical (Figure S7). Subsequently, G/MoS_2/Ag-4 yielded 2.5 times higher I_{ph}/I_{dark} value than G/MoS_2. Photoconversion efficiency (η) was estimated using the following equation to further quantify PEC performance:[34]

$$\eta = J(E^o - V_{app})/P_{light},$$

where J is the photocurrent density (mA/cm^2) at the applied potential, E^o is the standard reversible potential (1.23 V), V_{app} is applied potential, and P_{light} is the power density of illumination. The photoconversion efficiencies of Ag-decorated MoS_2 samples were significantly higher than that (0.8% at −0.45 V) of G/MoS_2 (Figure 8b). Among the samples, G/MoS_2/Ag-4 exhibited the highest photoconversion efficiency of 1.6% at −0.35 V. The photoconversion efficiency of G/MoS_2/Ag-4 further increased to 2.2% at −0.58 V in 0.5 M Na_2SO_3 + 0.5 M Na_2SO_4. The photoconversion efficiency G/MoS_2/Ag-4 was comparable with those of previously reported photoanodes, such as Au-decorated MoS_2 flakes on carbon fiber cloth (1.27%),[35] MoS_2 nanosheets on TiO_2 nanorods (0.81%),[36] Ag-embedded MoS_2/$BiVO_4$ heterojunctions (2.67%),[37] and MoS_2 nanosheets on polydopamine-modified

TiO_2 nanotubes (1.56%).[38] A significant amount of gas bubbles was observed from the photoanode (MoS_2) and the dark cathode (Pt) during PEC measurement (inset of Figure 7c), suggesting that the photocurrent can be attributed to the water-splitting reaction. Moreover, the photocurrents of G/MoS_2 and G/MoS_2/Ag-4 did not change significantly after 1,500 s of illumination, whereas the photocurrent of ITO/MoS_2 decreased continuously (Figure 8c). The photocurrents of G/MoS_2 and G/MoS_2/Ag-4 decayed initially but saturated shortly above 300 s. The decayed photocurrent was attributed to the recombination of the photogenerated holes with electrons.[39] The photocurrent became stable as the transfer and generation of photogenerated e–h pairs reached equilibrium. The stable photocurrent suggests the effective separation and transfer of the photogenerated e–h pairs in the heterojunction of graphene/MoS_2 nanosheets.

4. Conclusion

Plasmonic Ag-decorated vertically aligned few-layer MoS_2 nanosheets were prepared on graphene in a practical manner through MOCVD of MoS_2 and thermal evaporation of Ag. G/MoS_2 showed up to four times higher I_{ph}/I_{dark} than ITO/MoS_2 because of the efficient separation and transportation of the photo-generated carriers by the graphene/2D MoS_2 heterojunction. The PEC activity of G/MoS_2 was further enhanced by plasmonic Ag NP decoration. G/MoS_2/Ag-4 yielded 10 times higher I_{ph}/I_{dark} value than ITO/MoS_2. The maximum photoconversion efficiency of G/MoS_2/Ag-4 was 2.2% at −0.58 V. The significantly improved PEC performance was attributed to the synergetic effects of SPR and graphene/2D MoS_2 heterojunction. Plasmonic Ag NPs enhanced visible-light and near-IR absorption of 2D MoS_2, resulting in significantly increased the photo-generation rate of e–h pairs. Subsequently, the e–h pairs were efficiently separated and transported to catalytic surfaces across the favorable graphene/2D MoS_2 heterojunction and along the highly conductive edges of the vertically aligned 2D MoS_2, thereby significantly enhancing the PEC activity. This study offers a practical large-scale

approach that combines the potential of SPR and graphene/2D MoS_2 heterojunction effects for efficient PEC applications.

Acknowledgements

This research was supported by Basic Science Research Program through the National Research Foundation of Korea (NRF) funded by the Ministry of Education (2019R1I1A3A01059493 and NRF-2019R1A6A3A13095792).

References

1 M. G. Walter, E. L. Warren, J. R. McKone, S. W. Boettcher, Q. Mi, E. A. Santori, N. S. Lewis, *Chem. Rev.*, 2010, **110**, 6446–6473.

2 Q. Ding, B. Song, P. Xu, S. Jin, *Chem*, 2016, **1**, 699–726.

3 B. Han, Y. H. Hu, *Energy Sci. Eng.*, 2016, **4**, 285–304.

4 Chen, Y. Meng, J. Sha, C. Zhong, W. Hu, N. Zhao, *Nanoscale*, 2018, **10**, 34–68.

5 H. Li, Q. Zhang, C. C. R. Yap, B. K. Tay, T. H. T. Edwin, A. Olivier, D. Baillargeat, *Adv. Funct. Mater.*, 2012, **22**, 1385–1390.

6 K. F. Mak, C. Lee, J. Hone, J. Shan, T. F. Heinz, *Phys. Rev. Lett.*, 2010, **105**, 136805.

7 C. Lee, H. Yan, L. E. Brus, T. F. Heinz, J. Hone, S. Ryu, *ACS Nano*, 2010, **4**, 2695–2700.

8 H. He, J. Lin, W. Fu, X. Wang, H. Wang, Q. Zeng, Q. Gu, Y. Li, C. Yan, B. K. Tay, C. Xue, X. Hu, S. T. Pantelides, W. Zhou, Z. Liu, *Adv. Energy Mater.*, 2016, **6**, 1600464.

9 T. N. Trung, D. B. Seo, N. D. Quang, D. J. Kim, E. T. Kim, *Electrochim. Acta*, 2018, **260**, 150–156.

10 D. B. Seo, S. Kim, T. N. Trung, D. J. Kim, E. T. Kim, *J. Alloys Compd.*, 2019, **770**, 686–691.

11 Chang, Z. Mei, T. Wang, Q. Kang, S. Ouyang, J. Ye, *ACS Nano*, 2014, **8**, 7078–7087.

12 F. Carraro, L. Calvillo, M. Cattelan, M. Favaro, M. Righetto, S. Nappini, I. Píš, V. Celorrio, D. J. Fermín, A. Martucci, S. Agnoli, G. Granozzi, *ACS Appl. Mater. Interfaces*, 2015, **7**, 25685–25692.

13 R. K. Biroju, D. Das, R. Sharma, S. Pal, L. P. L. Mawlong, K. Bhorkar, P. K. Giri, A. K. Singh, T. N. Narayanan, *ACS Energy Lett.*, 2017, **2**, 1355−1361.

14 Z. Huang, W. Han, H. Tang, L. Ren, D. S. Chander, X. Qi, H. Zhang, *2D Mater.*, 2015, **2**, 035011.

15 X. Yu, R. Du, B. Li, Y. Zhanga, H. Liu, J. Qu, X. An, *Appl. Catal. B*, 2016, **182**, 504–512.

16 W. Zhou, K. Zhou, D. Hou, X. Liu, G. Li, Y. Sang, H. Liu, L. Li, S. Chen, *ACS Appl. Mater. Interfaces*, 2014, **6**, 21534−21540.

17 S. Linic, P. Christopher, D. B. Ingram, *Nat. Mater.*, 2011, **10**, 911–921.

18 S. Zu, B. Li, Y. Gong, Z. Li, P. M. Ajayan, Z. Fang, *Adv. Optic. Mater.*, 2016, **4**, 1463–1469.

19 A. Ali, F. A. Mangrio, X. Chen, Y. Dai, K. Chen, X. Xu, R. Xia, L. Zhu, *Nanoscale*, 2019, **11**, 7813–7824.

20 Y. Shi, J. Wang, C. Wang, T.-T. Zhai, W.-J. Bao, J.-J. Xu, X.-H. Xia, H.-Y. Chen, *J. Am. Chem. Soc.*, 2015, **137**, 7365−7370.

21 Y. Kang, S. Najmaei, Z. Liu, Y. Bao, Y. Wang, X. Zhu, N. J. Halas, P. Nordlander, P. M. Ajayan, J. Lou, Z. Fang, *Adv. Mater.*, 2014, **26**, 6467–6471.

22 Y. Y. Li, J. H. Wang, Z. J. Luo, K. Chen, Z. Q. Cheng, L. Ma, S. J. Ding, L. Zhou, Q. Q. Wang, *Sci. Rep.*, 2017, **7**, 7178.

23 L. V. Nang, E. T. Kim, *J. Electrochem. Soc.*, 2012, **159**, K93−K96.

24 J. Jeon, S. K. Jang, S. M. Jeon, G. Yoo, Y. H. Jang, J.-H. Park, S. Lee, *Nanoscale*, 2015, **7**, 1688–1695.

25 C. Yim, M. O'Brien, N. McEvoy, S. Winters, I. Mirza, J. G. Lunney, G. S. Duesberg, *Appl. Phys. Lett.*, 2014, **104**, 103114.

26 L. Bai, X. Cai, J. Lu, L. Li, S. Zhong, L. Wu, P. Gong, J. Chen, S. Bai, *ChemCatChem*, 2018, **10**, 2107–2114.

27 P. Zuo, L. Jiang, X. Li, B. Li, P. Ran, X. Li, L. Qu, Y. Lu, *ACS Sustain. Chem. Eng.*, 2018, **6**, 7704−7714.

28 J. Zhu, Z. Wang, H. Yu, N. Li, J. Zhang, J. Meng, M. Liao, J. Zhao, X. Lu, L. Du, R. Yang, D. Shi, Y. Jiang, G. Zhang, *J. Am. Chem. Soc.*, 2017, **139**, 10216−10219.

29 J. D. Major, M. Al Turkestani, L. Bowen, M. Brossard, C. Li, P. Lagoudakis, S. J. Pennycook, L. J. Phillips, R. E. Treharne, K. Durose, *Nat. Commun.*, 2016, **7**, 13231.

30 G. Eda, H. Yamaguchi, D. Voiry, T. Fujita, M. Chen, M. Chhowalla, *Nano Lett.*, 2011, **11**, 5111–5116.

31 C. Burda, X. Chen, R. Narayanan, M. A. El-Sayed, *Chem. Rev.*, 2005, **105**, 1025–1102.

32 H. Lee, S. Deshmukh, J. Wen, V. Z. Costa, J. S. Schuder, M. Sanchez, A. A. Ichimura, E. Pop, B. Wang, A. K. M. Newqaz, *ACS Appl. Mater. Interfaces*, 2019, **11**, 31543−31550.

33 Y. J. Yu, Y. Zhao, S. Ryu, L. E. Brus, K. S. Kim, P. Kim, *Nano Lett.*, 2009, **9**, 3430–3434.

34 S. U. M. Khan, M. Al-Shahry, W. B. Ingler Jr., *Science*, 2002, **297**, 2243–2245.

35 X. Xu, G. Zhou, X. Dong, J. Hu, *ACS Sustain. Chem. Eng.*, 2017, **5**, 3829−3836.

36 Y. Pi, Z. Li, D. Xu, J. Liu, Y. Li, F. Zhang, G. Zhang, W. Peng, X. Fan, *ACS Sustain. Chem. Eng.*, 2017, **5**, 5175−5182.

37 Q. Pan, C. Zhang, Y. Xiong, Q. Mi, D. Li, L. Zou, Q. Huang, Z. Zou, H. Yang, *ACS Sustain. Chem. Eng.*, 2018, **6**, 6378−6387.

38 L. Zeng, X. Li, S. Fan, M. Zhang, Z. Yin, M. Tadé, S. Liu, *J. Power Sources*, 2019, **413**, 310–317.

39 S. J. A. Moniz, S. A. Shevlin, D. J. Martin, Z.-X. Guo, J. Tang, *Energy Environ. Sci.*, 2015, **8**, 731–759.

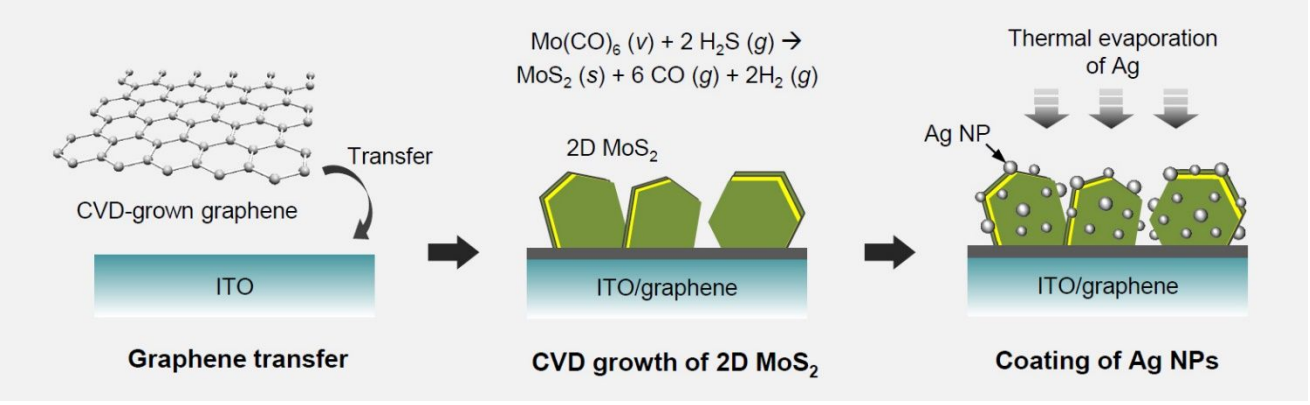

Figure 1. Schematic of preparation of plasmonic Ag-decorated vertically aligned few-layer MoS_2 nanosheets on graphene.

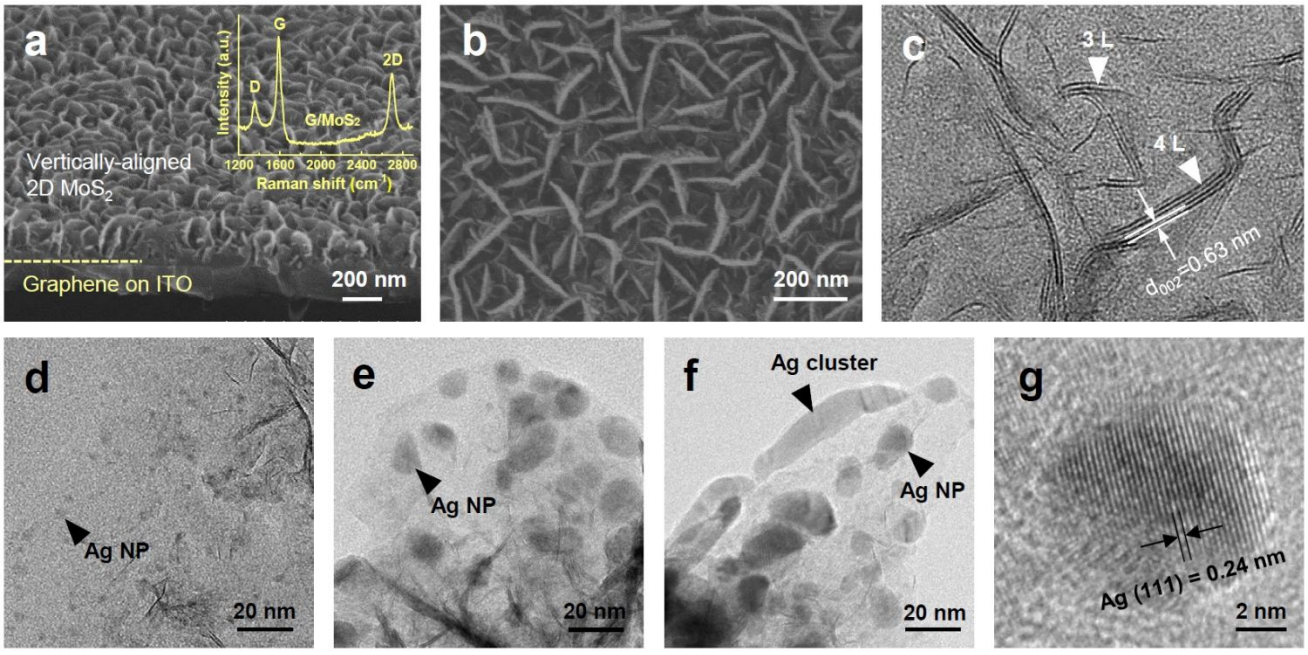

Figure 2. (a) Tilted-view SEM, (b) planar-view SEM, and (c) planar-view TEM images of vertically aligned MoS_2 nanosheets on graphene (G/MoS_2). The inset in (a) shows the Raman spectrum of G/MoS_2. TEM images of Ag-decorated vertically aligned few-layer MoS_2 nanosheets on graphene: (d) G/MoS_2/Ag-2, (e) G/MoS_2/Ag-4, and (f) G/MoS_2/Ag-8. (g) High-resolution lattice TEM image of an Ag NP in G/MoS_2/Ag-4.

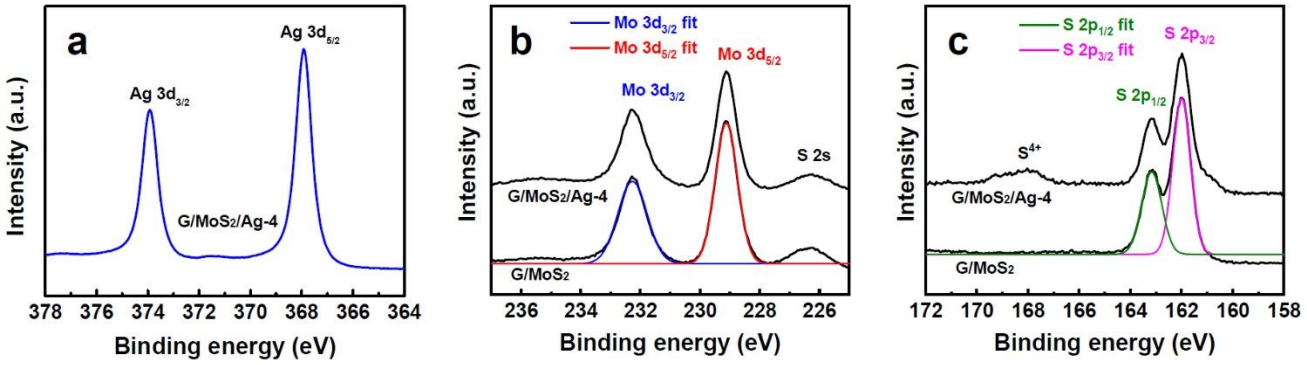

Figure 3. XPS spectra of (a) Ag 3d, (b) Mo 3d, and (c) S 2p core levels in G/MoS_2 and G/MoS_2/Ag-4.

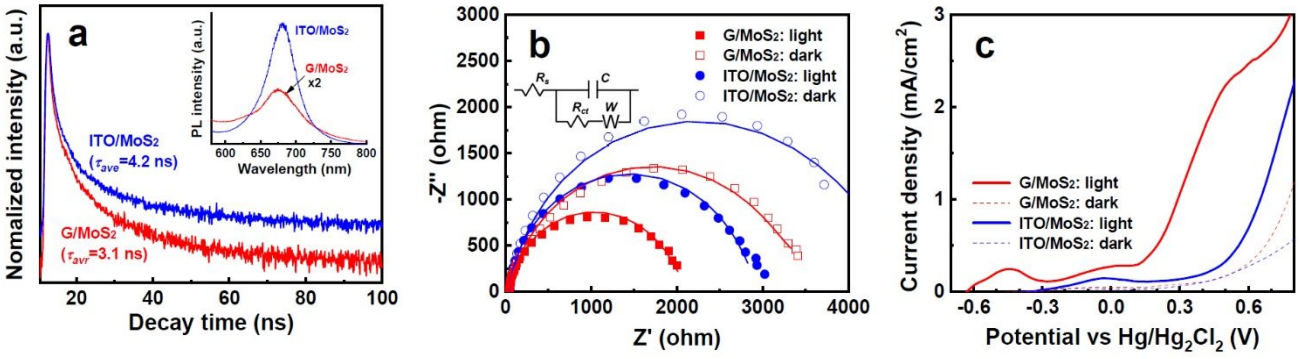

Figure 4. (a) TRPL results of ITO/MoS_2 and G/MoS_2. The inset shows the corresponding PL spectra. (b) Nyquist plots of ITO/MoS_2 and G/MoS_2 in the dark and under illumination. The inset shows the equivalent Randles circuit. (c) Photo and dark current densities versus the potential curves of PEC cells with working electrodes of ITO/MoS_2 and G/MoS_2.

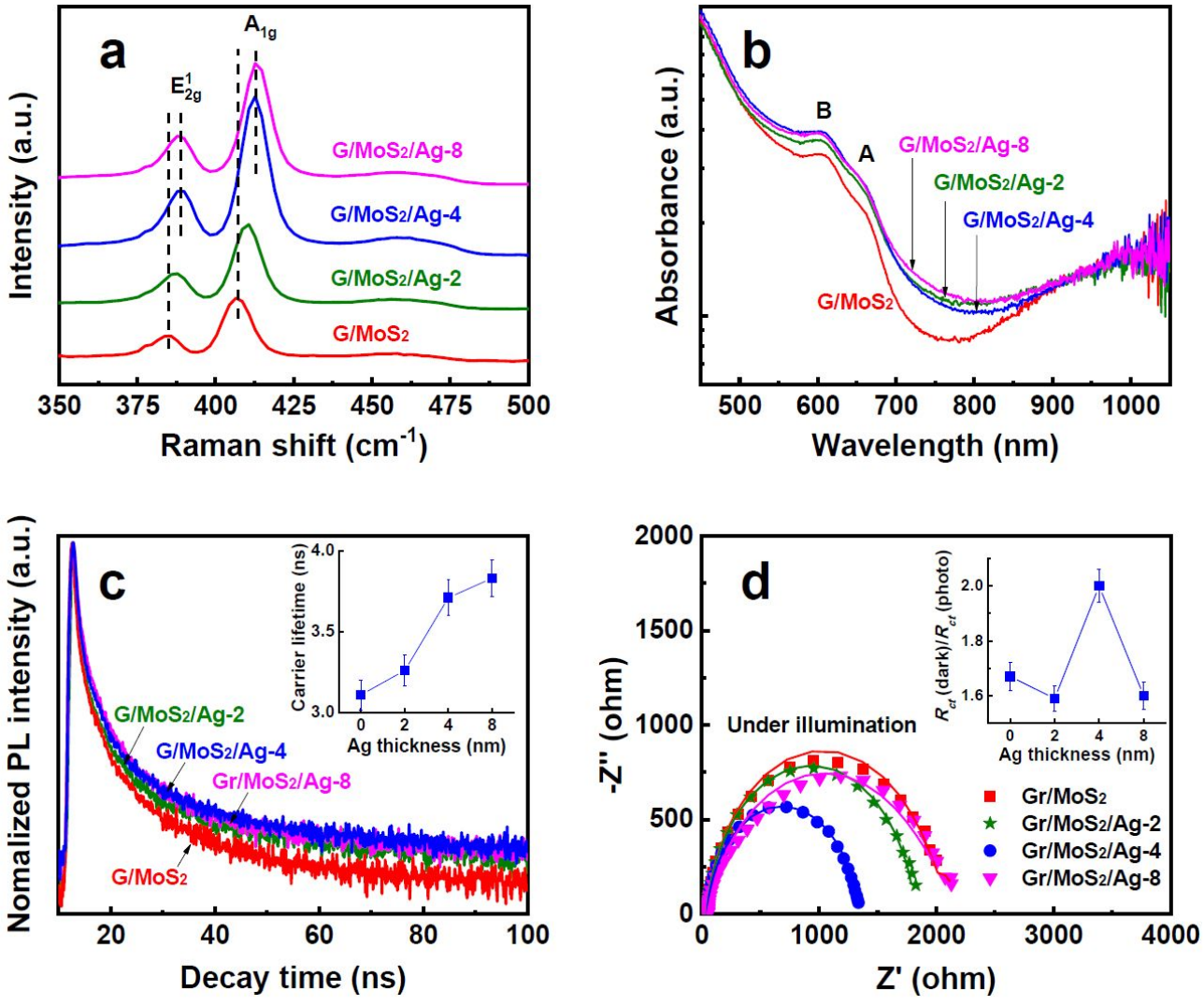

Figure 5. (a) Raman spectra, (b) UV–Vis absorption, (c) TRPL results, and (d) Nyquist plots of G/MoS_2, $G/MoS_2/Ag$-2, $G/MoS_2/Ag$-4, and $G/MoS_2/Ag$-8. The inset in (c) shows the carrier lifetimes based on the corresponding TRPL measurements. The inset in (d) shows the R_{ct} (dark)/R_{ct} (photo) values of G/MoS_2, $G/MoS_2/Ag$-2, $G/MoS_2/Ag$-4, and $G/MoS_2/Ag$-8.

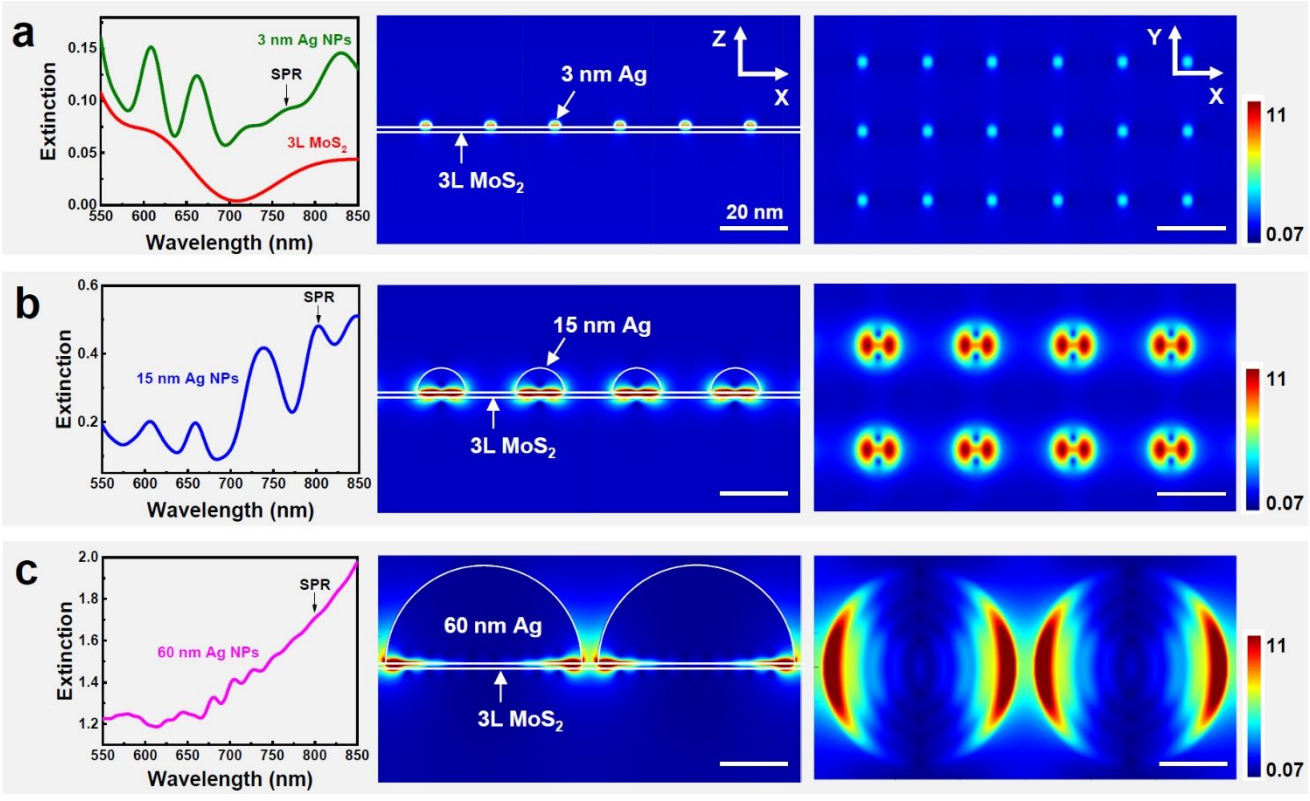

Figure 6. Simulated UV–Vis absorption spectra and electric field distribution contour plots at λ_{SPR} for (a) AgNP-3, (b) AgNP-15, and (c) AgNP-60.

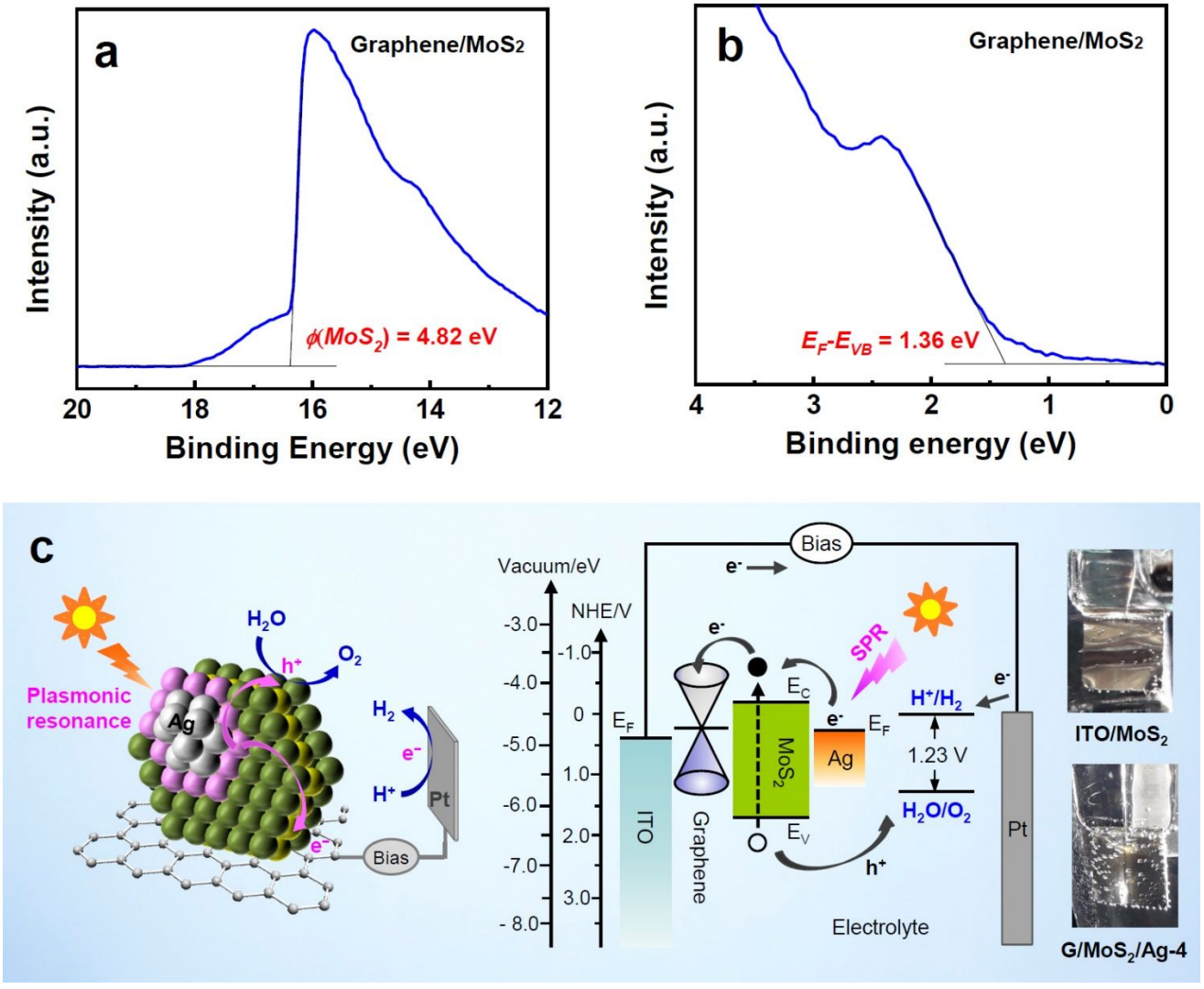

Figure 7. (a) UPS secondary electron cut-off and (b) valence spectra of G/MoS_2. (c) PEC water-splitting working principle of plasmonic Ag-decorated vertically aligned few-layer MoS_2 nanosheets on graphene. The photo images in (c) show gas bubbling on the dark cathodes (Pt) for ITO/MoS_2 and G/MoS_2/Ag-4 during PEC measurement.

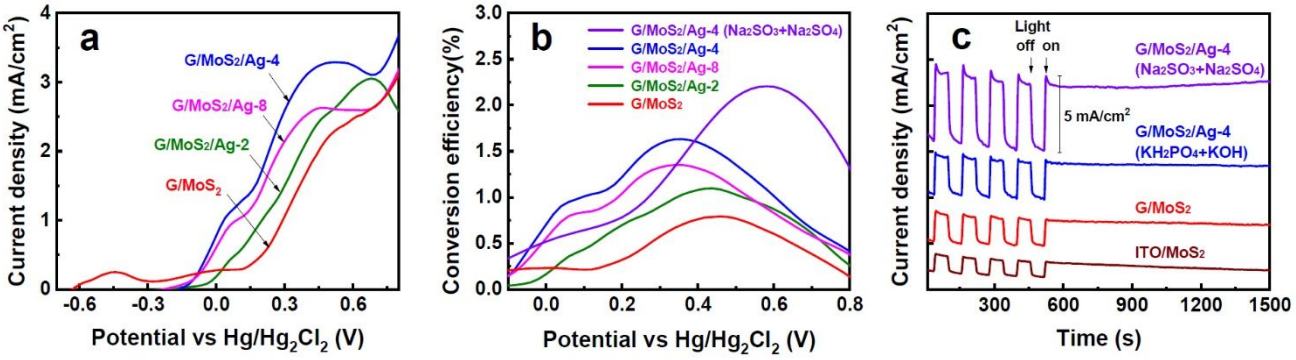

Figure 8. (a) Photocurrent density–potential curves of PEC cells with various working electrodes (G/MoS_2, G/MoS_2/Ag-2, G/MoS_2/Ag-4, and G/MoS_2/Ag-8) in 0.3 M KH_2PO_4 + 0.3 M KOH solution. (b) photoconversion efficiencies and (c) Photocurrent–time plots for G/MoS_2, G/MoS_2/Ag-2, G/MoS_2/Ag-4, and G/MoS_2/Ag-8 in 0.3 M KH_2PO_4 + 0.3 M KOH solution and G/MoS_2/Ag-4 in 0.5 M Na_2SO_3 + 0.5 M Na_2SO_4 solution.

Plasmonic Ag-Decorated Few-Layer MoS_2 Nanosheets Vertically Grown on Graphene for Efficient Photoelectrochemical Water Splitting

Dong-Bum Seo, Tran Nam Trung, Dong-Ok Kim, Duong Viet Duc, Jong-Ryul Jeong, and Eui-Tae Kim

The synergistic effects of surface plasmon resonance and favorable graphene/MoS_2 heterojunction is realized by a controllable and practical large-scale approach to enhance the photoelectrochemical reactivity of two-dimensional MoS_2.

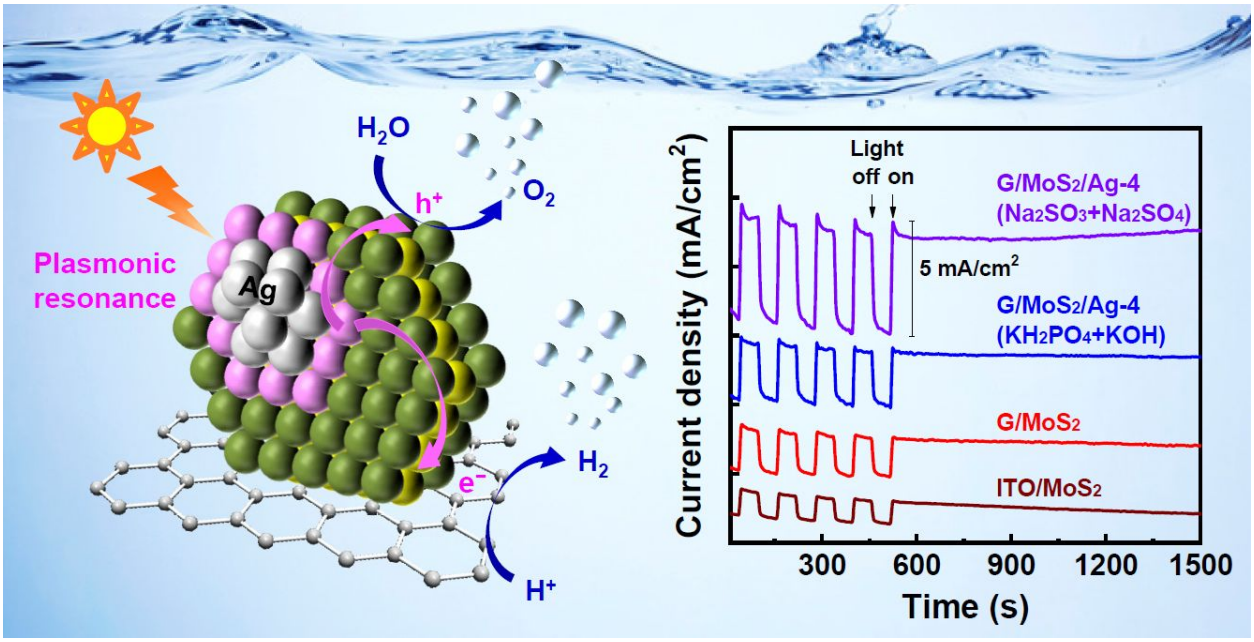

Supporting Information

Plasmonic Ag-Decorated Few-Layer MoS_2 Nanosheets Vertically Grown on Graphene for Efficient Photoelectrochemical Water Splitting

Dong-Bum Seo, Tran Nam Trung, Dong-Ok Kim, Duong Viet Duc, Jong-Ryul Jeong, and Eui-Tae Kim*

Department of Materials Science & Engineering, Chungnam National University, Daejeon 34134, Republic of Korea

* Corresponding author. E-mail: etkim@cnu.ac.kr

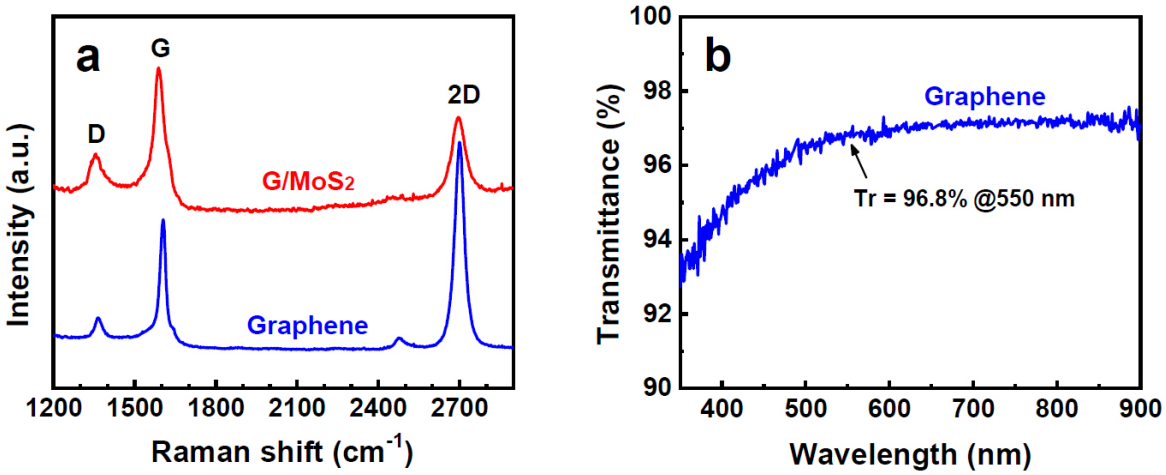

Figure S1. (a) Raman spectra of pristine graphene and G/MoS_2. (b) UV–Vis absorption spectrum of pristine graphene, exhibiting light transmittance of 96.8 % at 550 nm.

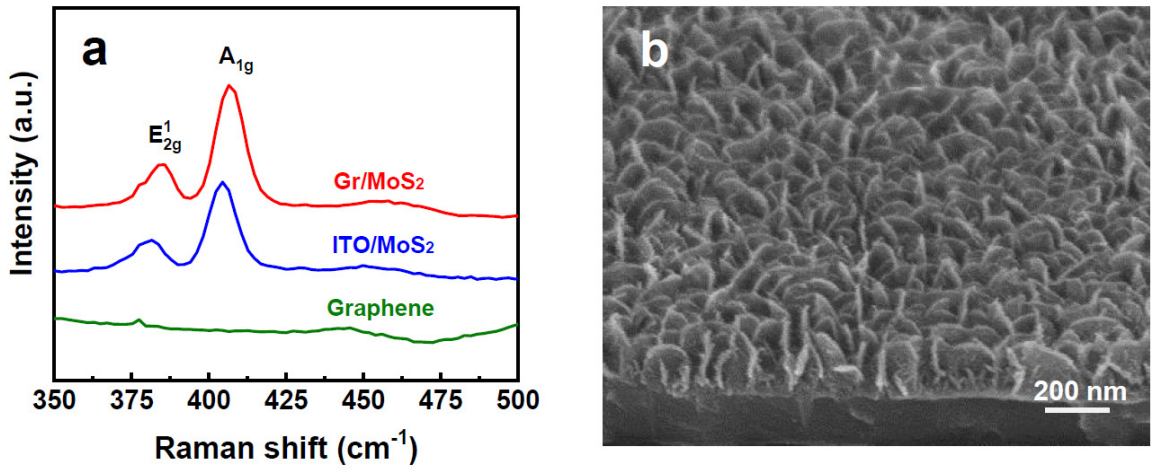

Figure S2. (a) Raman spectra of pristine graphene, ITO/MoS_2, and G/MoS_2. (b) SEM images of few-layer MoS_2 nanosheets grown on ITO (ITO/MoS_2).

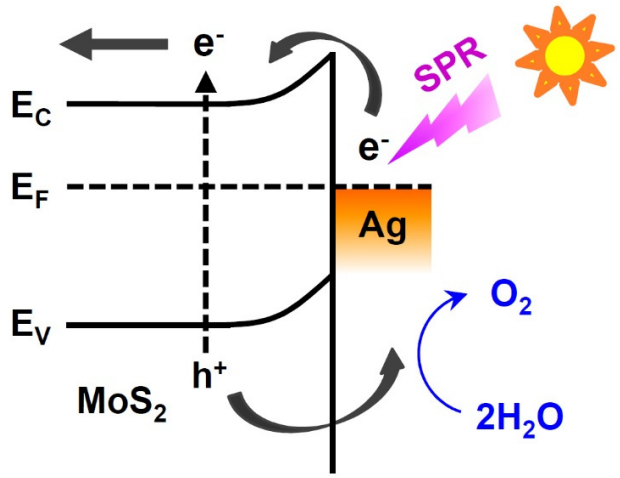

Figure S3. Energy band diagram of the Schottky junction of MoS_2/Ag.

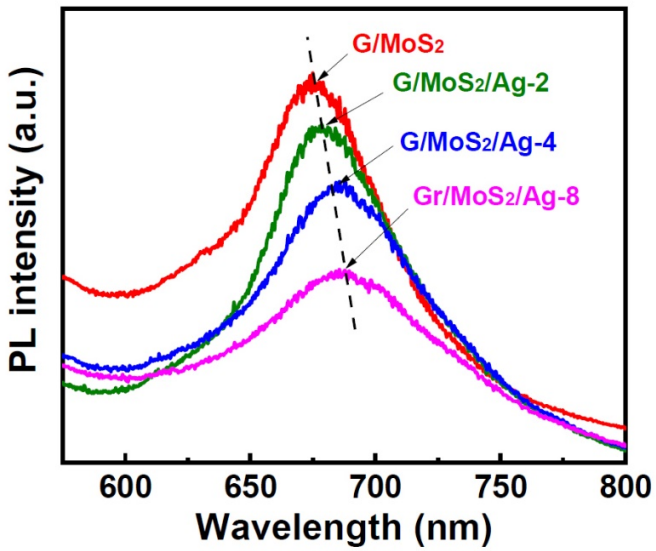

Figure S4. PL spectra of G/MoS_2, G/MoS_2/Ag-2, G/MoS_2/Ag-4, and G/MoS_2/Ag-8.

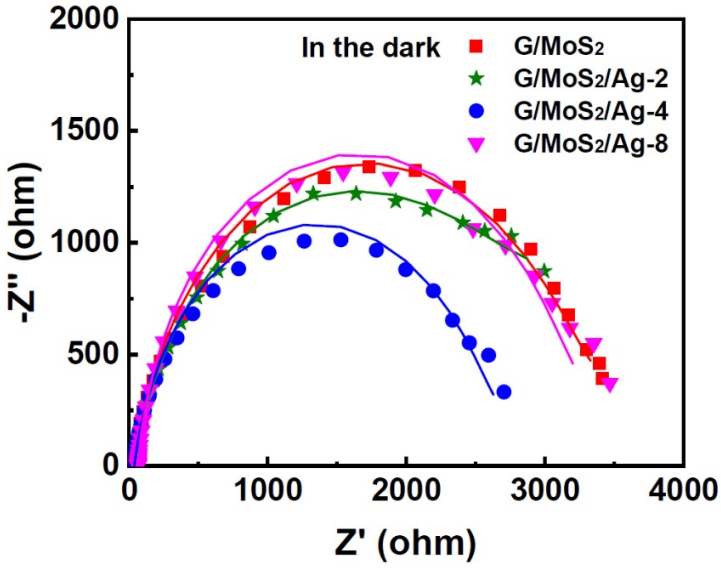

Figure S5. Nyquist plots of G/MoS_2, G/MoS_2/Ag-2, G/MoS_2/Ag-4, and G/MoS_2/Ag-8 in the dark.

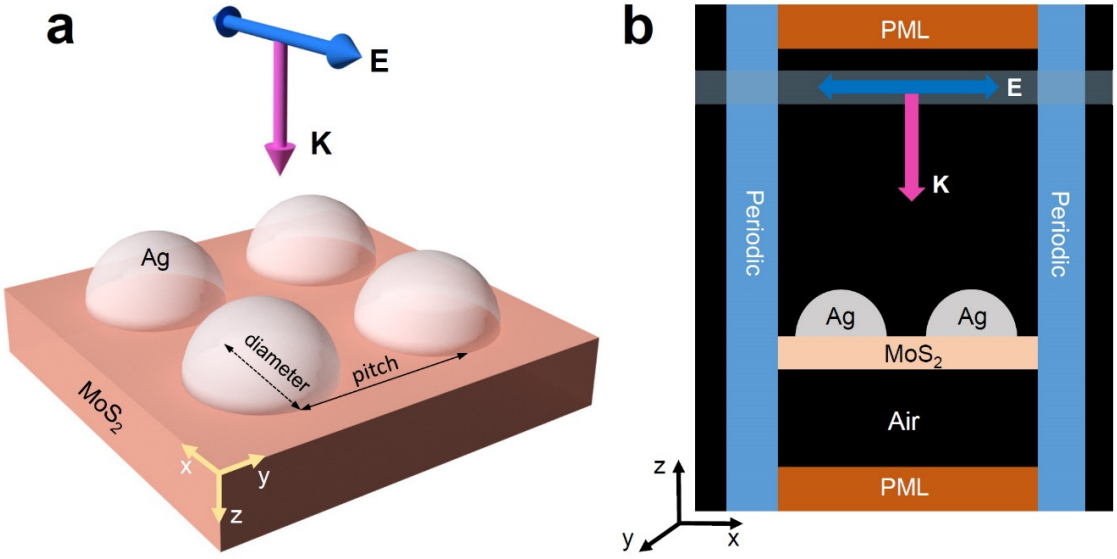

Figure S6. (a) Schematic representation of the formulated structure for FDTD simulations. The Ag NPs on a three-layer-thick MoS_2 substrate is irradiated by a plane-wave source with the propagation vector in the *z*-direction and the E-field oscillating along the *x*-axis. (b) Real simulation environment with applied periodic boundary conditions.

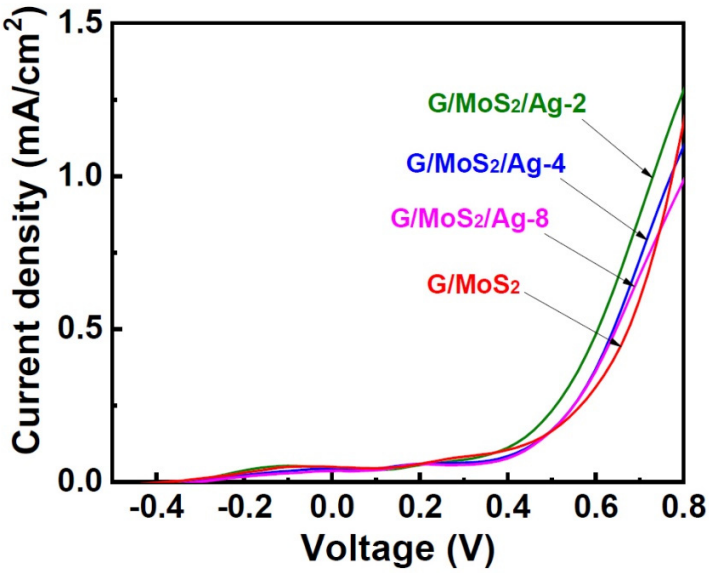

Figure S7. Dark current density–potential curves of PEC cells with various working electrodes (G/MoS_2, G/MoS_2/Ag-2, G/MoS_2/Ag-4, and G/MoS_2/Ag-8).

Table S1. R_{ct} and R_s values of EIS analysis in the dark and under illumination.

Samples	Dark		Illumination		
	R_{ct} [Ω]	R_s [Ω]	R_{ct} [Ω]	R_s [Ω]	R_{ct} (dark)/R_{ct} (photo)
ITO/MoS_2	4236	43.7	2766	45.5	1.53
G/MoS_2	3264	40.1	1959	40.2	1.67
G/MoS_2/Ag-2	2834	41.7	1780	41.7	1.59
G/MoS_2/Ag-4	2572	40.2	1284	44.2	2.00
G/MoS_2/Ag-8	3110	66.8	1947	48.3	1.60